Kinematic Analysis of the Solar ind Using Rotating Electric Fields

Masanao Hotta

Office TANDEM L.L.C

Corresponding author: Masanao Hotta (sam.hotta@nethome.ne.jp)

Key Points:

Measurement by rotating electric fields enables the identification of multiple ions in the solar wind retaining their initial charge state.

An incident ion beam is separated into multiple beams by lateral electric forces, marking patterns on an image sensor in order of velocity.

The proposed instrument is equipped with units to perform an energy analysis, an overall velocity analysis and a detailed velocity analysis.

Abstract

This paper describes a method for analyzing the kinematic properties of ions composing the solar wind. The core technology is a velocity analysis performed by dual rotating electric field (REF) units arranged coaxially in tandem, where the electric field in the downstream unit is set in the opposite direction to the upstream one. When the solar wind flies freely through the REF units, ions diverge outwards in the upstream unit and converge inwards in the downstream unit. Since the degree of diversion and conversion correspond to each ion's velocity, ions separate into multiple groups flying through the REF units, terminate their flights on an image sensor placed on the tail end, and create sorted patterns that exhibit the velocity distribution of ions. As the REF units act on ions only by dynamic lateral electric force, the initial velocity and charge state of the ions remain invariant during the analysis process, which can be advantageous for solar wind analysis. This paper introduces a proposed instrument equipped with multiple functions, including an energy analysis, an overall velocity analysis, and a detailed ion velocity analysis. The kinematic properties of the measured ions correspond to energy levels ranging from 300 eV to 20 keV, velocities from 20 km/s to 1,900 km/s, and mass numbers from 1 to 200.

Plain Language Summary

An extremely fast flow of ions and electrons called the solar wind, which could fly between New York and Paris in 15 seconds, constantly erupts from the sun. Although a magnetic sector mass spectrometer can measure the velocity of such high-speed ions on Earth, it is too heavy to be launched into space. This paper introduces a simple and lightweight ion velocity analyzer utilizing either a single or systemized dual rotating electric field(s). In the latter, ions enter and fly through the analyzer, are subjected to perpendicular forces from the rotating electric fields, and are separated according to velocity. By adjusting the rotational frequency of the fields, specified ions exit from the center of the outlet to be distinguished from other ions by speed. An improved analysis procedure

for the solar wind measurement not only selects specified ions but also identifies adjacent elements in one measurement to reduce the total measuring time. A velocity analysis in basic experiments and mathematical simulations confirmed that this analyzer is a powerful tool for kinematic elucidation of the solar wind. Even though numerous instruments with various features and functions have been implemented in space, this lateral approach is worthy of study.

1 Introduction

The solar wind consists of charged particles emitted from the sun at velocities ranging from 300 km/s to 800 km/s (Hathaway, 2014) carrying a tremendous amount of information about the sun's activity, which is crucial for determining the heliosphere's boundary. Many attempts to elucidate solar wind dynamics have been carried out over six decades, accumulating data and experience to update our knowledge (Asbridge et al., 1976; Bame, 1972; Bame et al., 1968; Feldman et al., 1976; Kallenbach et al., 1997; Marsch, E., 2006; Neugebauer, M., 2002; Parker, 1961; von Steiger et al., 1995). Numerous in-situ instruments to analyze charged particles in the solar wind have been placed into space, and they have been sending large volumes of data including energy, velocity, abundance ratio, isotopic ratio, and charge state distribution statistics (Bame et al., 1968; Bochsler et al., 1996; Crowther et al., 2012; Geiss, 1972; Gloeckler et al., 1995; Hundhausen et al., 1967; Ipavich, F., 1997; Kallenbach et al., 1997; Kasper et al., 2015; Leske, R., 1997; Mason et al., 1998; Mukai et al., 1987; Oglivie & Wilkinson, 1969; Shearer et al., 2014; Von Steiger et al., 2001) The majority of these analyses are based on a combination of energy analysis by a spherical analyzer and time of flight (TOF) analysis using carbon foil as an incident marker. From a physical point of view, however, it is difficult to maintain an initial charge state through the measurement process (Bochsler et al., 2000). In this respect, rotating electric field(s) (REF(s)) have a specific advantage in analyzing ions without mechanical interference.

Historically, Kramer and Poole carried out a mass analysis experiment by REFs in 1953 (Kramer & Poole, 1954). They created REFs using two X-Y deflectors, injected ions of different velocities into the deflectors, found that the ions travel along different courses in the downstream unit corresponding to their flight time difference between the two deflectors, and obtained a photograph of multiple ring patterns of different radii on a fluorescent plate set on the tail end. Although quantitative analysis was not described, the possible confirmation of mass separation by REFs was a great breakthrough. In 1998, Clemmons and Herrero reported experiments and analyses of ion interactions against a REF (Clemmons & Herrero, 1998). Using mathematical operations of ion arrival time, position on the detector, and phase angle of the REF, they obtained a spectrum. Their analyzer was launched into space in 2011 to collect new findings about the distribution of molecular species in ionospheric plasma.

In 2012, the author and his colleague started an inspection of a lightweight mass analyzer without using a magnetic sector, and elucidated a new method to perform ion velocity analysis using dual REF units that were systematically

activated and aligned in tandem (Hotta & Adachi, 2014). In 2013, a project group began experiments subsidized by JST (Japan Science and Technology Agency) to verify the theory, and in 2015, we succeeded in separating specified ions from others as a result of the systematic behavior (Ohwaki et al., 2005) of two REFs. In the experiment, we confirmed that a Ga ion beam was separated into two beams, a $_{69}$Ga+ beam and $_{71}$Ga+ beam, and obtained a velocity distribution spectrum by measuring the current of ions ejected from the center of the downstream unit sweeping the rotational frequency. This means that by selecting an arbitrary length and frequency of the units, the velocity analysis of ions flying at any speed is practicable. For example, if each length of the REF unit is 800 mm, by sweeping the frequency from 100 kHz to l MHz, a velocity spectrum from 80 km/s to 800 km/s is obtained. In addition to this essential feature, an improved function to select and read not only the centered ions but also other ions together was contrived. A preliminary instrument assembled from dual REF units and several ion optical components analyzes the ions while maintaining the initial charge state, which is a unique and promising feature that can determine the nature of the solar wind. Similar to a windsock swelling to reveal wind force and direction on Earth, a set of dual REF units can hover in the solar wind to read its velocity distribution. In this paper, the following issues are reported:

Physical and mathematical investigation of basic features of a single REF unit and dual REF units.

Report on a velocity/mass spectrometry experiment of Ga ions using dual REF units.

Introduction of the proposed instrument for solar wind analysis.

Simulation of an energy analysis, an overall velocity analysis, and a detailed velocity analysis by the proposed instrument.

2 Theory and methodology

2.1 Investigation of ion motion in the case of a single REF unit

The motion of an ion in an electric field can be expressed by the following equation:

$$m\frac{\mathrm{dv}}{\mathrm{dt}} = \mathrm{qE}, \quad (1)$$

where m is the mass of an ion (kg), v is the velocity (m/s), t is the time (s), q is the unit charge, and E is the electric field strength (V/m). The equation of motion in a REF with rotational angular velocity is calculated, assuming the X-axis as the horizontal direction, the Y-axis as the vertical direction, and the Z-axis as the central axis of rotation, thus,

$$m\frac{\mathrm{dv}_x}{\mathrm{dt}} = \mathrm{qE}\cos(\,\mathrm{t} + \theta_0), \quad (2)$$

$$m\frac{\mathrm{dv}_y}{\mathrm{dt}} = \mathrm{qE}\sin(\,\mathrm{t} + \theta_0)\,, \quad (3)$$

are obtained, where v_x is the velocity in the X-direction, v_y is the velocity in the Y-direction, and θ_0 is the initial phase angle of the REF. The value of angular velocity is obtained by multiplying the rotational frequency f by 2 . Therefore, the rotational speed is often characterized by the frequency f instead of angular velocity in this paper Integration of Eqations (2) and (3) gives

$$\frac{dx}{dt} = \frac{qE}{m}\{sin(\omega t + \theta_0\ ) - sin(\theta_0\ \ )\}, \quad (4)$$

$$\frac{dy}{dt} = \frac{qE}{m}\{-cos(\omega t + \theta_0\ ) + \cos(\theta_0)\}. \quad (5)$$

These equations explain the movement of an ion perpendicular to the flying direction. Integrating Eqations (4) and (5), the following equations are obtained:

$$x = \frac{qE}{m\omega^2}\{\ -cos(\omega t + \theta_0\ ) + \cos(\theta_0) - \ t\sin(\theta_0)\}, \quad (6)$$

$$y = \frac{qE}{m\omega^2}\{-\sin(\omega t + \theta_0\ ) + \sin(\theta_0) + \ t\cos(\theta_0)\}. \quad (7)$$

Eqations (6) and (7) and the following equation:

$$z = vt \qquad (8)$$

describe the ion's motion. These equations imply that the ions entering the REF follow cycloidal curves flying toward the exit and that their distances from the central axis or deviation,

$$r = \sqrt{x^2 + y^2}, \quad (9)$$

increase continuously. The equations also indicate that the amount of ionic deviation depends on the rotational frequency.

By assuming that the length of the REF unit is 800 mm, the deviation dependency of 11 groups of 10 keV ions differing in velocity/mass was estimated by sweeping the rotational frequency from 1 kHz to 10 MHz, as shown in Figure 1. The X-axis represents the frequency, and the Y-axis represents the amount of deviation marked on an

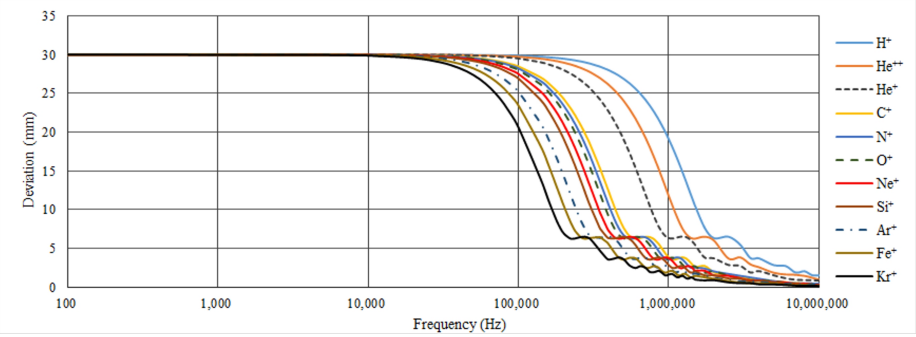

Figure 1. Deviation dependency of different velocity ions on frequency in a single REF unit. Deviation by an 800mm length REF unit was estimated with 11 kinds of 10 keV ions; the deviation of the lowest velocity Kr^+ (152 km/s)

decreases in frequency from 20 kHz to 189 kHz, and that of the highest velocity H^+ (1,390 km/s) decreases from 110 kHz to 1,740 kHz.

image sensor placed 100 mm at the rear. Although all ions show almost the same deviation below 10 kHz, that of slow-velocity ions begins to decrease above 20 kHz, and the majority of ions show a decrease in deviation between 100 kHz and 1 MHz. The ion's transit time through the unit and the period of the REF are comparable in this frequency range, so the difference in deviation due to the velocity is distinguishable. To clarify, Figure 2 shows the result of another simulation in the case of a rotational frequency of 189.459 kHz. The values of deviation are 29 mm for protons, 24 mm for carbon, 22 mm for Ne, 15 mm for Ca, and 8 mm for Kr. These values correspond to each radius of circular patterns, depicting the abundance of each ion as luminescence intensity, formed by ion beams on the image sensor. This procedure constitutes the single REF analysis. Since mass numbers from 1 to 84 are distributed within 21 mm, ion separation is attainable, although identification may be challenging. Figure 3 shows

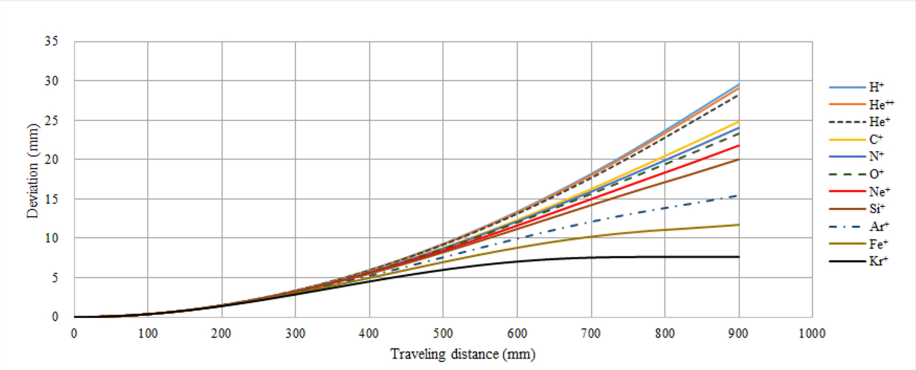

Figure 2. Deviation dependency on velocity/mass difference in a single REF unit. Fixing the frequency of the REF at 189.459 kHz, deviation of 11 kinds of 10 keV ions was estimated. H^+ depicts the top side curve and Kr^+ the bottom side one, showing velocity/mass dependency. Kr^+ shows a noteworthy flight, which is parallel to the center axis after passing the REF unit.

the orbits of ions forming cycloidal curves viewed from the incident point. The slight difference in deviation in Figure 2 is amplified in Figure 3, implying the possibility of intensifying the accuracy of velocity analysis if the relationships among the arrival time, arrival position to the detector, and phase angle of the REF unit are fully grasped.

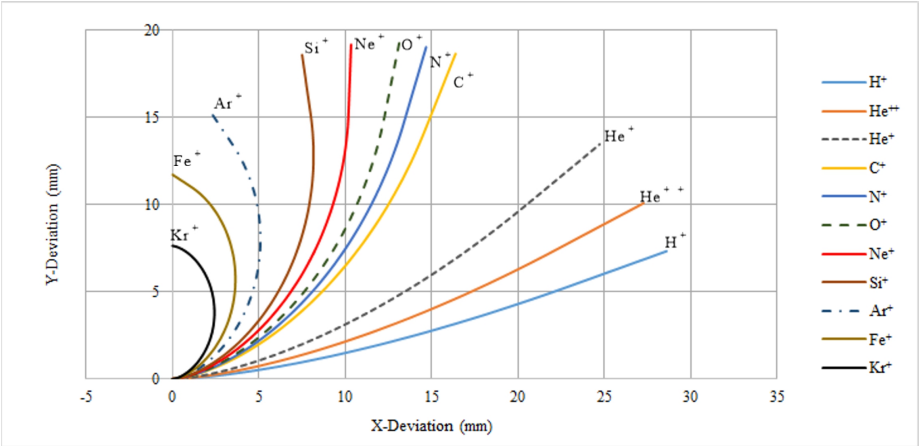

Figure 3. Trajectories viewed from the incident point of a single REF unit. Each ion except Kr follows a portion of a cycloidal curve. Only Kr completes a cycloidal curve.

In Figure 2, the Kr ion appears to be flying parallel to the central axis after exiting the unit. This is because the frequency of the unit is selected to match the traveling time of Kr $^+$ through the REF unit, which transforms t into 2 at the exit of the REF unit and Eqations (4) and (5) into null as a consequence, meaning that this ion has no component of deviation. The ions that travel through the unit in just one rotational period are named index ions; their velocity is the index velocity, and the rotational frequency is the index frequency. In the above example, Kr^+ is the index ion, with an index velocity of 151.567 km/s and an index frequency of 189.459 kHz. Figures 2 and 3, which are obtained from Eqations (2) to (9), indicate that after exiting the unit, only the index ions fly parallel to the central axis, while other ions fly with some inclination toward the axis. This argument leads to the idea of arranging one more REF unit coaxially in the downstream direction so that only the index ions are returned onto the central axis and that other ions do not converge onto the central axis. In the following section, the orbits of ions when using dual REF units are examined mathematically.

2. 2 Investigation of ion motion in the case of dual REF units

Two REF units are arranged coaxially in tandem, and a sinusoidal wave with the same amplitude and frequency is applied. The rotational frequency of the downstream REF unit is shifted by 180 degrees from the upstream unit so that the ions experience a reverse electric force. When the index ions leave from the upstream REF unit, Eqations (4) to (7) are expressed as follows:

$\frac{dx}{dt} = 0$, (10)

$\frac{dy}{dt} = 0$, (11)

$x = \frac{-qE}{m\omega^2} \{2\pi \sin(\theta_0)\}$, (12)

$y = \frac{qE}{m\omega^2} \{2\pi \cos(\theta_0)\}$. (13)

The ions entering from the center deviate from the central axis and exit in parallel to the central axis from the circle obtained by Eqations (12) and (13). When another REF unit with a phase angle shifted by 180 degrees is placed in a downstream position, ions entering the downstream unit at positions obtained by Eqations (12) and (13) are subjected to the opposite force from the electric field, and

$\frac{dx}{dt} = \frac{-qE}{m}\{sin(\omega t + \theta_0\ ) - sin(\theta_0\ \ )\}$, (14)

$\frac{dy}{dt} = \frac{-qE}{m}\{-cos(\omega t + \theta_0\ ) + \cos(\theta_0)\}$, (15)

$x = \frac{-qE}{m}\{\ -cos(\omega t + \theta_0\ ) + \cos(\theta_0) -\ t\sin(\theta_0)\} - \frac{qE}{m\omega^2}\{2\pi \sin(\theta_0)\}$, (16)

$y = \frac{-qE}{m}\{-\sin(\ t + \theta_0) + \sin(\theta_0) +\ t\cos(\theta_0)\} + \frac{qE}{m\omega^2}\{2\pi cos(\theta_0)\}$, (17)

are obtained. When the index ions leave the downstream unit, the motion is calculated as follows:

$\frac{dx}{dt} = 0$, (18)

$\frac{dy}{dt} = 0$, (19)

$x = 0,$ (20)

$y = 0.$ (21)

Eqations (18) to (21) state that the index ions surely return to the central axis and proceed along this axis. However, ions with other velocities cannot return and deviate from the central axis at a distance corresponding to each velocity. Figure 4 shows an orbital simulation of an ion beam composed of five adjacent different velocity ions where the median velocity ions are chosen as the index. The red lines represent trajectories of index ions, the green

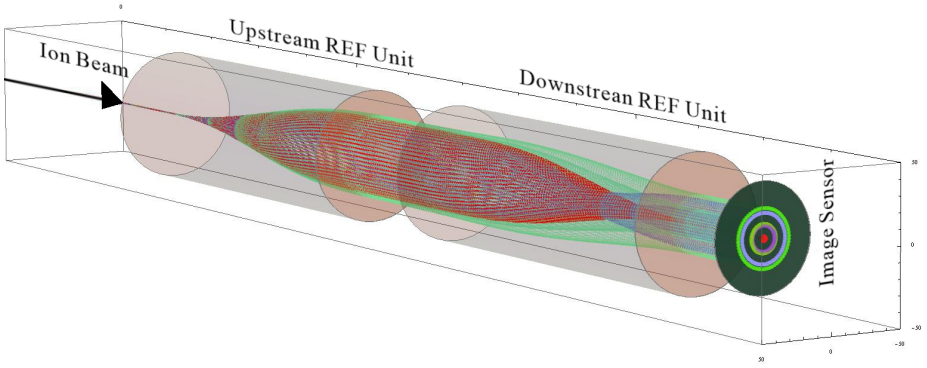

Figure 4. Trajectories and projected patterns obtained by a simulation with ions of five adjacent velocities. When the median velocity ions are assigned as index ions, they are projected onto the center position, while other ions form

circular patterns overlapping each other. Therefore, only the centered ions can be identified.

lines represent faster ions, the purple lines represent slower ions, and the pale brown cylindrical regions denote the REFs. First, incident ions are diffused in a cone shape in the upstream unit, separated in progress corresponding to each velocity, and exit the upstream unit in cylindrical or cone shapes. After flying through free space, the ions enter the downstream unit and converge toward the central axis under the influence of a reversed electric field. Only index ions exit from the center in the shape of a zero-radius cylinder or a solid beam to form a spot on the center of the image sensor, whereas other ions exit the unit in multiple cylindrical shapes of radii corresponding to their velocities, forming annular patterns. When the diameter of the spot is smaller than the nearest outer annular radius, the index ions can be visually separated from other ions. Although there are adjacent annuli of one-step slower ions (purple) and faster ions (green) surrounding the red dot (the center spot) in Figure 4, it is difficult to distinguish these annuli clearly because they almost overlap each other. Furthermore, two-step slower ions (purple) and faster ions (green) appear around these rings. Although they are clearly separated in Figure 4, the separation may be degraded depending on the beam diameters. As a result, a spectrum can be obtained by measuring the current of centered ions by sweeping the frequency of the REF units. Thus, a velocity analysis using dual REF units is verified.

3 Experiment

A joint group of 3 universities and 2 companies conducted experiments to verify the above theory from 2013 to 2015. Figure 5 shows a set of dual REF units activated in the experiments. The photograph on the left shows a cross section of the REF unit composed of 8 electrodes in a circular arrangement with an inner radius of 10 mm; this view shows the entry location of incident ions. The right side shows a side view of the analyzer, where two 150 mm length REF units are assembled in tandem spacing of 70 mm between the two. We connected this device to an ion

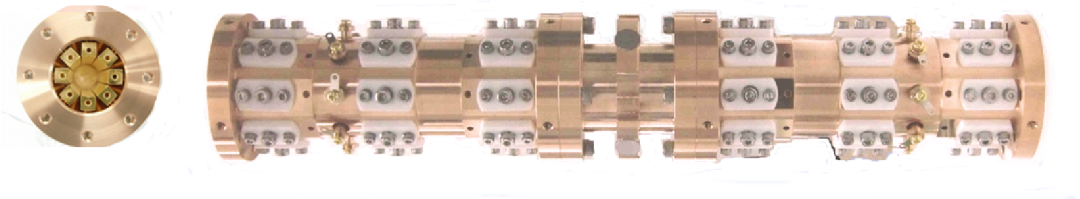

Figure 5. View of a set of dual REF units. Inlet view (left) showing eight electrodes in the housing and side view (right) showing the 150 mm upstream REF unit, 70 mm interspace, and 150 mm downstream REF unit.

optical column equipped with a 10 keV field emission ion gun sharing the central axis. For the ion source, we chose liquid Ga which contains isotopes $_{69}$Ga and

$_{71}$Ga that travel at velocities of 167.323 km/s and 164.948 km/s respectively. An ion beam was emitted from the gun and was controlled to focus to a beam diameter of approximately 200 m on the image sensor. Passing through the set of dual REF units, the ion beam was separated in accordance with each velocity. The separated beams collided against the image sensor with a fluorescent surface placed at the tail end and terminated their flights in the form of bright annular patterns, signifying the velocity information of ions. Figure 6 shows the image of Ga isotopes separated on the image sensor (Nojima et al., 2016). As each index frequency was estimated to be 1,115 kHz for $_{69}$Ga and 1,100 kHz for $_{71}$Ga from experimental conditions, the dual REF units were activated at frequencies ranging from 1,080 kHz to 1,125 kHz. When the frequency was swept between these ranges, separated Ga ion orbits formed characteristic patterns on the image

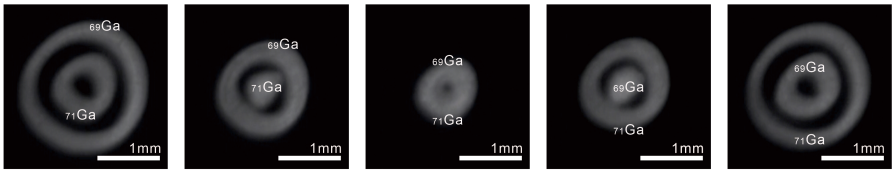

Figure 6. Dependency of projected radius of $_{69}$Ga and $_{71}$Ga on the rotational frequency of the REF units. The pattern radius initially decreases as the rotational frequency increases, reaches a minimum at each index frequency, and then monotonically increases. $_{71}$Ga ions show the minimum at 1,097 kHz [image (b)]; $_{69}$Ga ions show the minimum at 1,112 kHz [image (d)].

sensor. Figure 6 (a) shows the result at a frequency of 1,087 kHz; $_{69}$Ga generates an annulus pattern with a radius of 900 m and $_{71}$Ga generates an annulus pattern with a radius of 340 m. Image (b) shows the case of 1,097 kHz where $_{71}$Ga is focused on the center and $_{69}$Ga forms an annulus pattern with a radius of 540 m around it. Image (c) shows the case of 1,104 kHz, where both annuli overlap. Image (d) shows the case of 1,112 kHz where $_{69}$ Ga converges and $_{71}$Ga generates a circle with a radius of 520 m around it. Image (e) shows the case of 1,122 kHz, where the outer ring is $_{71}$Ga and the inner ring is $_{69}$Ga. This serial phenomenon indicates that the radius of the annulus decreases as the rotational frequency approaches the index frequency, becomes null when they coincide, and

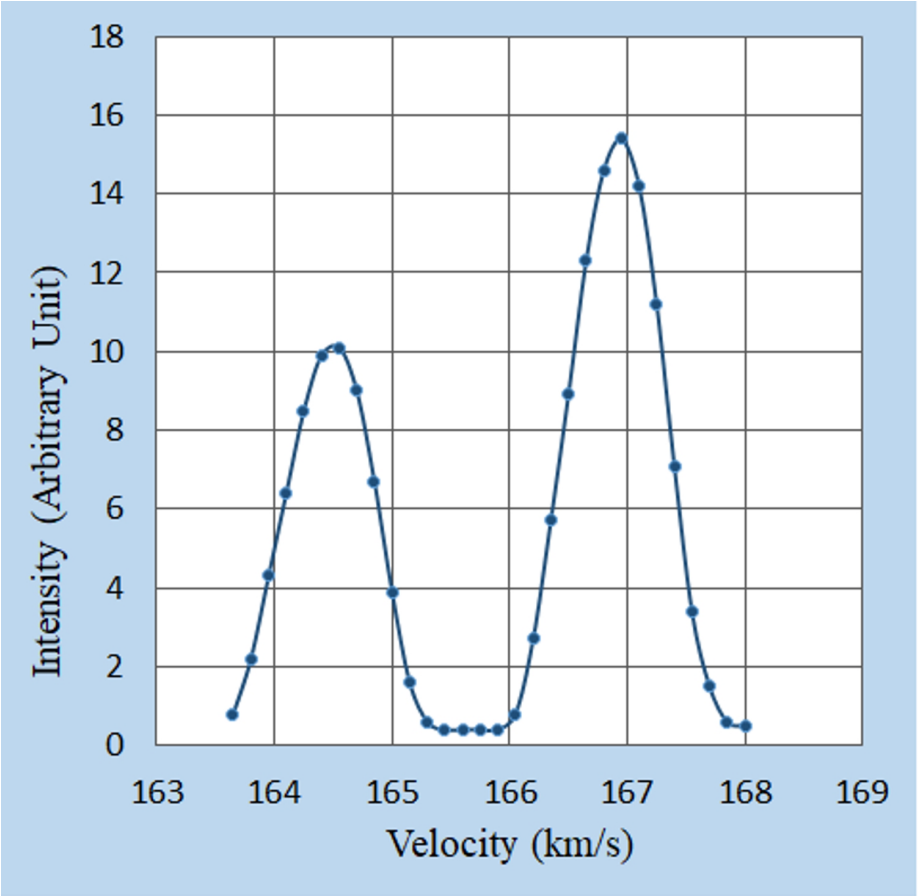

Figure 7. Velocity distribution of 10keV Ga ions obtained by the dual REF units. The X-axis represents velocity converted from rotational frequency. The left peak corresponds to $_{71}Ga^{+}$, and the right peak corresponds to $_{69}Ga^{+}$.

expands when the frequency exceeds the index frequency. Figure 7 shows the velocity distribution of the ion beam where the X-axis represents the velocity converted from the rotational frequency. The ions of 164.948 km/s ($_{71}$Ga) and 167.323 km/s ($_{69}$Ga) are clearly separated at a resolution of 180. With the X-axis representing the mass number converted from the frequency, the graph illustrates the mass spectrum (Anai et al., 2016). Note that the frequencies adopted in the experiments were shifted to the lower side by 0.23% compared to the calculated value. This peak shift was caused by the leakage of the electric field from both REF units, which is unavoidable. Despite this minor discrepancy, the overall result is consistent with the calculation, confirming the reliability of the theory. Moreover, this analyzer showed excellent capability in analyzing high-mass elements such as $_{197}$Au (Nojima, 2017). This feature was also verified in mass ranges exceeding 100,000 such as argon cluster ions aggregated from

over a thousand monomers (Moritani et al., 2018). These experiments were supported by the Advanced Equipment Development Program of JST.

4 Proposed instrument under consideration for solar wind analysis

4.1 Solar wind analysis utilizing REF unit(s)

In the first experiment described in Section 3, Ga isotopes with velocities of 165 km/s and 167.3 km/s were separated clearly by a set of dual REF units without energy analysis because the ion beam energy was determined by the ion source potential. In addition, the Ga ion beam was well-collimated to a half apex angle of less than 0.011 degrees with a diameter of 200 m and a density as high as 10^{10} ions/s on the image sensor. On the other hand, to kinematically analyze the solar wind using dual REF units, some preprocessing is indispensable prior to REF analysis since the values of kinematic parameters are considerably diffused and dispersed.

It has been reported that the mass range of ions in the solar wind is distributed from 1 for H to 136 for Xe (Bame, 1972; Zurbuchen, 1998; Growther et al., 2012), with energy levels ranging mainly from 300 eV to 4 keV exibiting a peak at 1 keV in terms of protons, velocities ranging from 280 km/s to 870 km/s (Bame, 1972; Zastenker & Borodkova, 1991), angular dispersion of flying direction ranging by +/- 10 degrees (Hundhausen et al., 1967; Mukai et al., 1987), ion flux ranging from $3x10^8$ to $3.8x10^8$ ion/cm^2 /s at 1 AU (Ryden, 2011; Zastenker & Borodkova,1991), and charge states distributed from +1 to +14 (Bame, 1972; Ipavich, 1997). To analyze the solar wind, it is necessary to shape an ion beam by separating the dispersed excess part of the solar wind, selecting the specified energy ions, and maintaining a sufficiently fine beam diameter on the image sensor.

In the velocity analysis of Ga^+ by the dual REF units, a 150 mm length was chosen for each REF unit to analyze approximately 165 km/s ions. Since this length incurs excessive power consumption to activate the REF units compared to the estimation, an 800 mm length is considered suitable for 800 km/s ions of the solar wind, which calls for the total length of the analyzer, including a spherical analyzer, an electrostatic lens, a set of dual REF units, and an image sensor, to be approximately 5,000 mm. Although this total length, which is inevitable for measuring the high speed of the solar wind directly, might create excessive bulk, this concern can be mitigated by designing a foldable analyzer that can be packed within 1 cubic meter. From these physical dimensions, an appropriate beam diameter to be projected onto the image sensor is estimated. Since a 75 mm image sensor across is already available (Hamamatsu Photonics K.K. 2021), a beam of 7 mm across is considered to be reasonable. To visualize such a beam on the image sensor, two countermeasures are needed. One is to restrict the half apex angle to 0.03 degrees to keep the beam narrow while traversing the analyzer. Another is to restrict the half apex angle to 0.7 degrees so that the beam does not impinge against any electrode or the chamber wall and focuses the dispersed beam into a prescribed diameter on the image sensor

by arranging an electrostatic lens. In the case of 0.03 degrees, 2 ions/s collide with the image sensor, whereas in the case of 0.7 degrees, approximately 1,500 ions/s collide on average. To perform an efficient analysis, the latter is advisable. By counting ion beam dispersion and degradation due to the aberration of ion optical systems, a preferable incident beam should have a diameter of 5 mm, which is obtained by passing the beam through an aperture. If the instrument stated above is constructed and appropriate electrical signals are applied to the electrodes, REF analysis of the solar wind can be implemented. In both cases—single and dual REF analysis—annular patterns of various radii are obtained on the image sensor depicting ion velocity differences. In the case of dual REF analysis, specified ions or index ions are ejected from the center of the outlet and separated from the others. In the previous theoretical description of dual REF units, only the ions projected on the center of the image sensor were identified, whereas surrounding ions were ignored (Figure 4). Additionally, in experiments, only the centered ions were measured to obtain a velocity spectrum (Figure 7). This is a regrettable factor, especially in the case of solar wind analysis. Since the solar wind is so dilute and dispersed, the measurement should be more efficient and panoptic if possible. For example, if a method to identify not only the index ions but also surrounding ions in one measurement is realized, it will open up new avenues. To address this issue, two methods are discussed in more detail below.

The first is a stroboscopic method, which is a common technique to virtually halt rotation and is suitable for a single REF analysis. In concrete terms, an ion beam taken out of the solar wind is packetized and synchronized to the electric field rotation by a beam deflector placed far ahead of the REF unit. Each constituent packet enters the REF unit at different times and different phase angles. These packets form dotted or small arc patterns lined in a spiral on the image sensor. The positions of the patterns depict the velocity distribution of the incident ion beam, and their luminance shows each level of abundance. Although the resolution of this method is not high, the kinematic properties of the solar wind can be obtained in one measurement. This method is discussed later.

The second is a silhouette method, which can be utilized for dual REF analysis. Since the ion beams exit the upstream unit in cylindrical or cone shapes, as shown in Figure 4, the beams are partially blocked by a partial beam stopper placed between the two units, while the remainder proceeds through the downstream unit to be projected on the image sensor, forming arc patterns. Neighboring ions of smaller mass numbers than the index ion (faster-speed group) form arc patterns at a short distance from the center on the image sensor. The missing parts of these patterns are the shaded part, or the "silhouette". Those of larger mass numbers than the index ion (slower-speed group) proceed with their flight along 180-degree rotated courses from the faster beams in the downstream unit and form similar arc patterns on the image sensor facing the faster group patterns across the center point. That is, these ions are projected onto the shaded part made by previous ions, creating invisible silhou-

ettes on previous arc patterns. As a result, the arc patterns of slower beams and faster beams than the index ion are projected on opposite sides and can be identified clearly, which is suitable for high-resolution analysis. A trajectory analysis of a silhouette method is shown in Figure 8. Arc patterns are projected on the image sensor and separated into two groups: a slow-speed

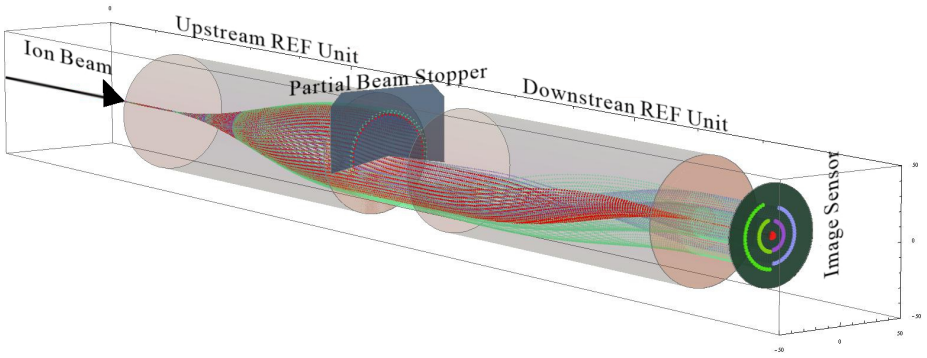

Figure 8 Trajectories and projected patterns obtained by a simulation with five ions of adjacent velocities in the case of a silhouette method. The physical conditions are the same as in Figure 4 except for a partial beam stopper. Surrounding the center point, arc patterns are shown in two groups. One is formed by ions slower than the index ion, and the other is formed by faster ions.

group (purple) and a fast-speed group (green). Since the velocity difference is reflected on each radius, ions that were difficult to distinguish from each other in Figure 4 are now clearly separated. Thus, all the ions composing the incident beam can be identified by a silhouette method. Note that the partial beam stopper in Figure 8 is 10% larger than a half disc to prevent the edges of arc patterns from overlapping each other, which occurs in the case of a half disc. Although it may appear inefficient to utilize less than half of the incident ion beam, the efficiency is improved as a result since five or more elements can be identified at the same time. Both a stroboscopic method and a silhouette method ensure successful use of the REF unit(s).

4.2 Proposed instrument for kinematic analysis of the solar wind

In summary, this analyzer is composed of beam deflecting units to control the passing and stopping of an incident beam, a spherical analyzer for energy analysis, an electrostatic lens for beam focusing, dual REF units for velocity analysis, a partial beam stopper to apply the silhouette method, an image sensor to detect ion arrival, and electronic circuit units with power supplies to control the electromechanical equipment. Figure 9 shows an example of the proposed analyzer. The solar wind enters from the inlet (first aperture) of the analyzer and flies through as an ion beam that is gradually separated, encountering electric forces from the field framed by multiple electrodes. Although most of these beams may collapse against the metal wall of the analyzer and disappear on

their way, those beams that meet specific conditions pass through the analyzer and collide with the image sensor, generating luminescent spots depending on their kinematic properties. The image sensor to be utilized in the system is a multichannel plate 75 mm across and with 90% conversion efficiency, which is sufficient to monitor the trajectory separation of ion

Figure 9. Configuration diagram of the proposed instrument. The instrument takes in the solar wind as an ion beam from the first aperture. A beam of specified energy is selected by the spherical analyzer, separated into plural beams according to velocity by a single or dual REF unit(s), and the beams terminate their flights on the image sensor. Labeled components are as follows: 1. First aperture, 2. First beam deflector, 3. Spherical analyzer, 4. Second aperture, 5. Second beam deflector, 6. Beam aligner, 7. Limiting aperture, 8. Electrostatic lens, 9. Upstream REF unit, 10. Partial beam stopper, 11. Downstream REF unit, 12. Image sensor.

beams 7 mm across. This analyzer accommodates three operational modes. The first mode is an energy analysis activating a spherical analyzer, electrostatic lens, and an image sensor to monitor the energy distribution in a range from 300 eV to 20 keV at +/- 1%. The second mode is an overall analysis of the velocity distribution between 20 km/s and 1,900 km/s, activating beam deflectors to packetize the ion beam and either the upstream or the downstream REF unit in addition to the first mode, to reveal the overall velocity distribution of the ion beam. The third mode is a detailed velocity analysis of multiple ions activating dual REF units and the partial beam stopper, to project the index ions and several neighboring ions separately onto the image sensor at a resolution over 100 in one measurement, providing crucial information for investigating the isotopic abundance ratio of the solar wind. These three different modes of analysis are readily prepared to be activated in a minute, providing effective measuring circumstances.

5 Simulation results of the proposed instrument

5.1 Energy analysis

The spherical energy analyzer consists of dual quadrant spheres concentrically set with different radii. To create an electric field toward the center of the sphere, different voltages are applied to each sphere. The radius of the center orbit in Figure 10 is 300 mm, and the energy resolution is +/- 1% for an ion beam of 5 mm across. An ion beam

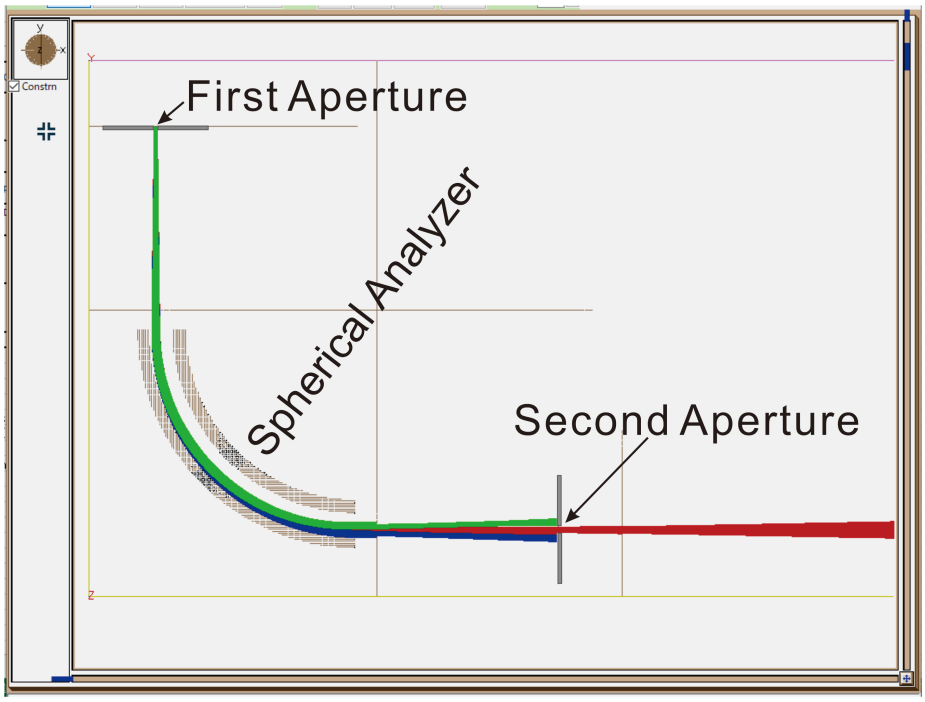

Figure 10. Energy analysis by a spherical analyzer. Trajectories of three different energy ions were verified in the simulation. The red beam energy is 5 keV, the green beam energy is 4.9 keV, and the blue beam energy is 5.1 keV.

enters the first aperture and experiences radial force from the spherical analyzer. Ions of specified energy trace the center course with a radius of 300 mm, whereas other energy ions fly off the center course. Since the spherical analyzer focuses the ions, specified ions are focused onto the second aperture as an energy filtered ion beam. Figure 10 shows the result of a simulation of three different energy ions passing the spherical analyzer. Only the red beam (5 keV) passed through the second aperture of 5 mm across, while the green (4.9 keV) and the blue (5.1 keV) beams collided against the second aperture plate. This is how the energy separation is implemented by the spherical analyzer.

5.2 Beam focusing by electrostatic lensing

The resolving power of the proposed instrument depends on the beam diameter projected on the image sensor. Assuming that the divergent half-angle of the beam is 0.7 degrees, a beam 5 mm across expands to 36 mm after a 1 m progression, which degrades the resolving power. To accommodate this situation, several pairs of annular electrodes with an inner diameter of 120 mm are arranged in front of dual REF units as an electrostatic lens to focus the expanded beam onto the image sensor. Figure 11 shows a simulation result of the beam trajectory in the proposed instrument, where the beam is analyzed by the spherical analyzer and focused by the electrostatic lens. As the beam diverges with a half apex

angle greater than 0.7 degrees after passing the second aperture, only the beam with a half apex angle less than 0.7 degrees is sorted by the limiting aperture and is focused to a spot with a diameter less than 7 mm on the image sensor. In addition, the simulation revealed that the transmission efficiency of the

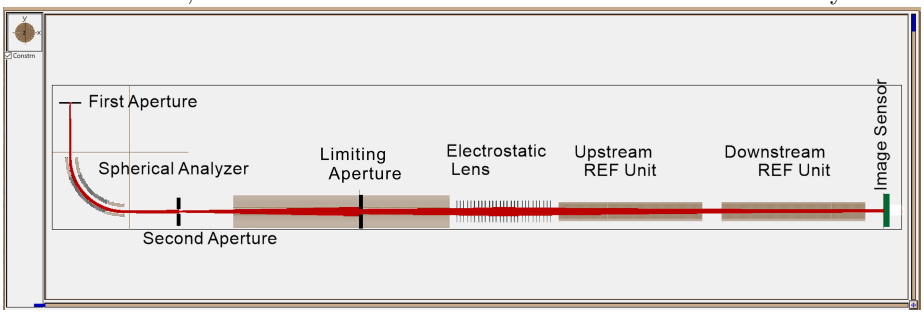

Figure 11. Focusing of the incident beam in the proposed instrument. An energy filtered beam is focused to 7 mm across on the image sensor with an electrostatic lens placed on the front of the two REF units. Both REF units are deactivated in this figure.

instrument is 60%, finally counting approximately 900 ions/sec on the image sensor. The performance of the electrostatic lens was confirmed by investigating the focused beam profile. Figure 12 illustrates a simulation result of the distribution of 900 ions that compose the 1 keV beam striking the image sensor for 1 second. The curves in the graph show the X and Y distributions. The graph reveals that the beam FWHM (Full width at half maximum) is

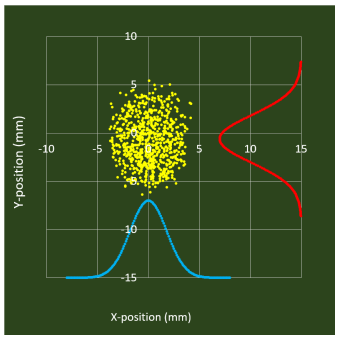

Figure 12. Ion distribution of a focused beam (1 keV) is illustrated with distribution curves showing the beam FWHM: 4.4 mm in the X-direction and 6mm in the Y-direction. Focusing characteristics show the same result at energy levels from 300eV to 20 keV.

4.4 mm in the X-direction and 6 mm in the Y-direction and that 81% of ions are included in this FWHM area. These properties were confirmed between energy levels ranging from 300 eV to 20 keV, indicating that the beam diameter remained under 7 mm or 1/10 of the diameter of the image sensor. Since no REF unit is activated in the case of Figure 11, the beam is not separated and

collides with the center of the image sensor. In this situation, by changing the voltage applied to the spherical analyzer and the electrostatic lens, an energy analysis is implemented by monitoring the centered beam.

5.3 Velocity analysis using REF unit(s)

5.3.1 Analysis for single REF unit activation

A simulation of a single REF analysis was performed by the proposed instrument activating the upstream REF unit of 800 mm length with an innerdiameter of 100 mm. The target of analysis was an ion beam composed of 13 elements already identified to be included in the solar wind and was filtered to 10 keV by the spherical analyzer The fastest group of ions was protons, at 1,389km/s, the slowest was Xe, at 122 km/s, with ions of He, C, N, O, Ne, Mg, Al, S, Ar, Fe, and Kr lining up in between. Figure 13 (a) illustrates annular patterns on the image sensor

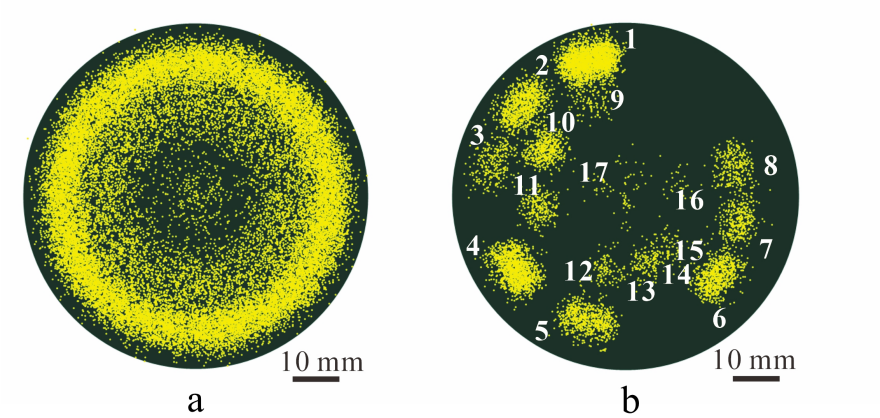

Figure 13. Simulated results activating a single REF unit: pattern obtained (a) with a continuous beam and (b) with a packetized beam.

Table 1. *The m/z and velocity of labeled ions shown in Figure 13 (b).*

Label No.	*m/z*	Velocity (km/s)
1	1	1,389
2	1.5	1,134
3	2	982
4	3	802
5	4	695
6	6	567
7	7	525
8	8	491
9	12	401
10	14	371

Label No.	m/z	Velocity (km/s)
11	16	347
12	20	311
13	22	296
14	23	290
15	24	284
16	28	263
17	40	220

indicating their velocity difference generated by a continuous beam. Protons are projected on the outermost annular pattern and slower elements on the inner annuli in turn when $_{56}$Fe was selected as the index ion and the upstream REF unit was activated with an index frequency of 232.039 kHz. Figure 13 (b) illustrates the result of a stroboscopic analysis visualizing an overall velocity analysis by the proposed instrument. The beam that is synchronously packetized to the REF unit enters and flies through the REF unit forming arc patterns spirally aligned on the image sensor. Each position of arc patterns indicates their velocity or m/z (m over z). The outermost pattern represents protons at 1,389 km/s, $_3$He^{++} at 1,134 km/s, $_4$He^{++} at 982 km/s, and so on. Table 1 shows the labeled m/z in Figure 13(b) and each velocity. In practice, it takes approximately 10 to 60 min to obtain a result, as shown in Figure 13 (b). Even though the separation is insufficient and the innermost part is blurred, a stroboscopic method has a distinct advantage in characterizing the kinematic properties of the solar wind.

5.3.2 Analysis for dual REF unit activation

A simulation of dual REF unit activation was implemented, where each unit has a length of 800 mm with an inner diameter of 100 mm. Figure 14 shows the result of an analysis of ions filtered to the 2 keV energy level. Both REF units were activated with an index frequency of 162 kHz for mass number 23 ions assigned as the index ion. Figure 14 (a) shows the result simulated with a continuous beam. Index ions are projected onto the image sensor's center

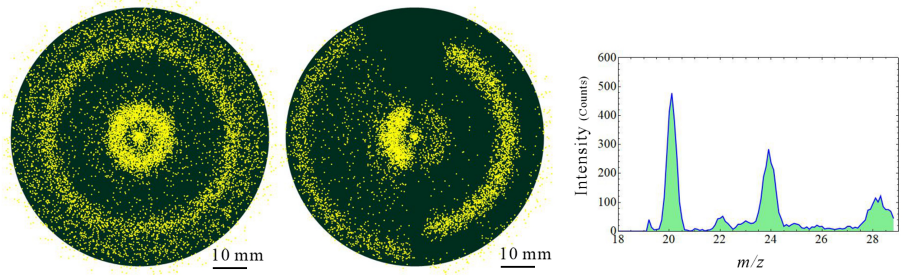

Figure 14. Simulated results activating dual REF units: (a) pattern obtained by

basic operation, (b) using a silhouette method; (c) mass spectrum derived from (b), where the X-axis represents the mass number transferred from frequency. Mass numbers from 20 to 28 correspond to velocities from 135.6 km/s to 117.4 km/s.

and bright concentric circles formed by neighboring ions surround the center spot. However, it is difficult to identify the elements from the surrounding concentric circles. To obtain accurate results, a silhouette method was developed. In this method, a partial beam stopper is placed between the two REF units to block a part of the ion beams flying in cylindrical or cone shapes. Unblocked ions keep flying, whereas blocked ions cast their silhouette on the image sensor. Unblocked ions are to be separated into two groups, a group slower and another faster than the index ion. These groups pass through the downstream REF unit, forming cycloidal curves with index ions between them, exiting the REF unit surrounding index ions, and colliding against the image sensor on the counterpart's silhouette. Since each group contains subgroups of ions different in velocity, each of them forms multiple arc patterns corresponding to their velocity. Figure 14 (b) illustrates the simulation results of a silhouette method visualizing a detailed velocity analysis by the proposed instrument, where, ions of $_{28}$Si (117.404 km/s), $_{27}$Al (119.558 km/s), $_{26}$Mg (121.836 km/s), $_{25}$Mg (124.248 km/s), and $_{24}$Mg (126.810 km/sec) are lined up from left to center, $_{23}$Na (129.538 km/s) is centered, and $_{22}$Ne (132.449 km/s), $_{21}$Ne (135.566 km/s), and $_{20}$Ne (138.914 km/s) are observed from center to right. Figure 14 (c) shows the abundance from mass number 20 to 28 in the solar wind deduced from Figure 14 (b); the X-axis represents m/z converted from frequency. The projected patterns in Figure 14 (a) overlap and are difficult to identify except for the index ion. On the other hand, those of Figure 14 (b) are all separated and can be identified. Although it might take a few hours to a few days to obtain an image, as shown in Figure 14 (b), the silhouette method provides indispensable information to identify neighboring elements of an index ion in one measurement.

5.4 Simulation conditions

Table 2 shows a summary of the operating conditions of each component used in the five simulations of Figures 11, 13 (a) and (b), and 14 (a) and (b). The components correspond to those of Figure 9. As shown in Figure 11, simulations of energy analysis and beam focusing were performed using SIMION©, which is a software package used to calculate the electric fields and trajectories of charged particles. Figures 13 (a) and (b) show the result of simulations of single REF analysis based on Equations (1) to (9), Figures 14 (a) and (b) show the result of simulations of dual REF analysis based on Eqations (1) to (21), both with the aid of *Mathematica*©.

Table 2. *Simulation Conditions of Components*

Components	Signals	Unit	Simulated figure numbers	
			Figure 11	Figure 13(a)

Components	Signals	Unit	Simulated figure numbers	
			First mode	
Beam Deflectors	Amplitude	V	Off	Off
	Frequency	Hz		
	Duty Ratio			
Spherical Analyzer	Inner Electrode	V	-180.6	-1,806
	Outer Electrode	V	150.0	1,500
Upstream REF Unit	Amplitude	V	Off	+/-28
	Frequency	Hz		232,039
Downstream REF Unit	Amplitude	V	Off	Off
	Frequency	Hz		
Lens	Voltage	V	689.8	6,898
	Sigma Value	mm	75	75
Ions	Energy	keV	1	10
	Mass	Da	1	1 to 129
	Velocity	km/s	982	122~1,389
Partial Beam Stopper	Off	Off	Off	On
Expected Measurement Time	<1 min	10 min	50 min	8 h
Software	SIMION©8.1	Mathematica©9		

Note; These simulations were performed with referring to earlier studies (Bame, 1972; Bochsler et al., 2000; Geiss,1972; Kallenbach et al., 1997; Mason G et al., 1997; Ogilvie & Wilkerson, 1969; von Steiger et al., 1995; Wimmer-Schweingruber, 1998; Zurbuchen et al, 1998)

5.5 Estimation of resolution

The resolution of this instrument was investigated numerically. Although the main feature of this instrument is velocity analysis, mass spectrometry takes place at a certain energy level. Therefore, it is appropriate to calculate the

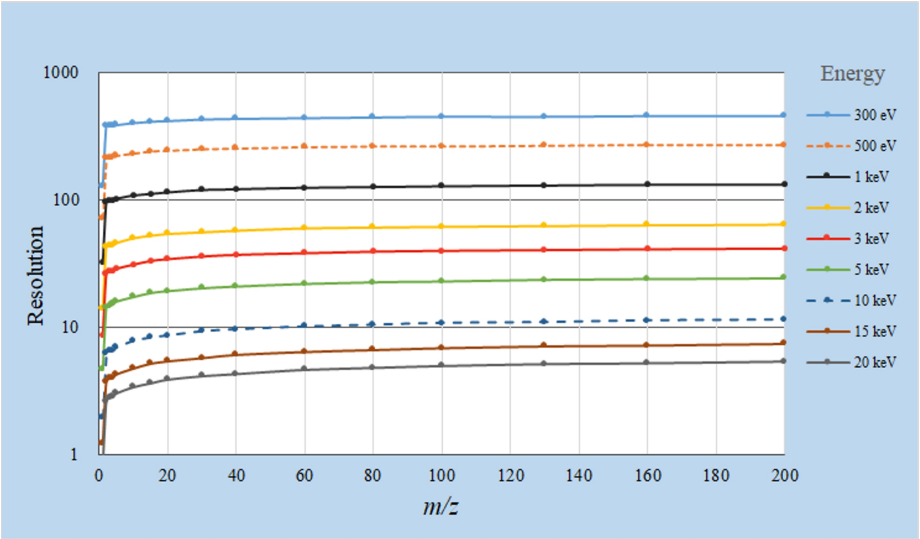

Figure 15. Estimation of the mass resolution. The graph shows values higher than 100 in the energy range from 500 eV to 1 keV.

resolving power as the mass resolution. This parameter is defined as the ratio obtained from the mass number divided by the half-width of the mass spectrum in question. In this paper, the resolution is estimated using 2.4 of the beam diameter instead of the FWHM of the peak. Figure 15 shows the resolution of the mass number from 1 to 200 at each energy level. Note that the resolution is high even in the small-mass-number region. It is comparatively low, however, in the high-energy level because of the low voltage amplitude of the REF units, which suppresses power consumption.

6 Conclusion

Solar wind has been a consistent candidate for investigation since the beginning of space exploration. In this paper, a theoretical explanation of the trajectory separation of ions by a single and a dual REF analysis was first reported. Next, experiments using dual REF units sorting out ions of specified kinematic properties were reported. Furthermore, a stroboscopic method for single REF analysis and a silhouette method for dual REF analysis were introduced to improve the functional capability of the analyzer identifying multiple ions simultaneously. On the basis of the theories and experiments discussed above, a proposed instrument was designed to provide an energy analysis, an overall velocity analysis, and a detailed velocity analysis aimed at kinematic analysis of the solar wind. Simulation results of trajectory separation by the instrument were fairly reasonable and convincing. Combining these three analyses, a 3D spectrum is obtained revealing the kinematic properties of the solar wind in detail: energy levels ranging from 300 eV to 20 keV, velocities ranging from 20 km/s to 1,900 km/s, and mass numbers ranging from 1 to 200. The time required for one measurement is estimated to be 1 to 2,000 min depending on abundance and aiming accuracy.

This REF(s) analyzer offers unique advantages in the kinematic analysis of ions and characterization of the behavior and composition of the solar wind.

7 Acknowledgments

The greatest driving force for writing this paper was the success of the experiments to evaluate the performance of dual REF units that took place from 2013 to 2015 supported by JST's Advanced Equipment Development Program. Many thanks to the comembers of the project group: Masashi Nojima (Tokyo University of Science), Kaoru Suzuki, Satoshi Kurumi (Nihon University), Kousuke Moritani (University of Hyogo), Tatsuya Adachi, and Takashi Kusanagi (Ampere Co., Ltd.) for their endeavors and fruitful results. Many thanks also to the graduate students from each university who contributed greatly to circuit designs and various experimental works. Finally, the author expresses his gratitude to K. Hotta (Office TANDEM L.L.C.) for her assistance in discussions, proofreading and a substantial incidental paperwork during the polishing of the dissertation corresponding to this work.

References

Anai, Y., Nojima, M., Hotta, M., Kurumi, S., Suzuki, K., Adachi, T., et al (2016). Development of mass spectrometer using two rotating electric fields for separation of high-mass ions, *e-journal of Surface Science and Nanotechnology,* 14, 161-164.

Asbridge, J. R., Bame, S. J., Feldman, W. C., Montgomery, M. D. (1976). Helium and hydrogen velocity difference in the solar wind, *Journal of Geophysical Research*, 81(16), 2719-2727.

Bame, J. (1972). Spacecraft observations of the solar wind composition, *Conference paper; NASA Conference held at Asilomar Conference Grounds, California, March 21-26,* 1971, 535-558.

Bame, S. J., Hundhausen, A. J., Asbridge, J. R., Strong, I. B. (1968). Solar Wind ion Composition, Physical Review Letters, 20 (8), 393-395.

Bochsler, P., Gonin, M., Sheldon, R. B., Zurbuchen, T., Gloeckler, G., Hamilton, D. C., et al (1996). Abundance of solar wind magnesium isotopes determined with WIND/MASS, *Proceedings of the Eighth International Solar Wind Conference,* N382, 199-202.

Bochsler, P., Ipavich, F. M., Paquette, J. A., Weygand, J. M., Wurz, P., (2000). Determination of the abundance of aluminum in the solar wind with SOHO/CELIAS/MTOF, *Journal of Geophysical Research*, 105(a6), 12,659-12,666

Clemmons, J. H. and Herrero, F. A. (1998). Mass spectroscopy using a rotating electric field, *Review of Scientific Instrument.* 69, 2285-2291.

Crowther, S. A., Gilmour, J. D., (2012). Measuring the elemental abundance and isotopic signature of solar wind xenon collected by the Genesis mission,

Journal of Analytical Atomic Spectrometry, 27 (2), 256-269.

Feldman, W. C., Asbridge, J. R, Bame, S. J., Gosling, J. T. (1976). High-speed solar wind flow parameters at 1AU, Journal of Geophysical Research, 81 (28), 5054-5060.

Geiss, J., (1972). Elemental and isotopic abundances in the solar wind, *conference paper, https://ntrs.nasa.gov/api/citations/19730002080/downloads/19730002080.pdf*

Gloeckler, G., Balsiger, H., Burgi, A., Bochsler, P., Fisk, L. A., Galvin, A. B., et al. (1995). The solar wind and suprathermal ion composition investigation on the wind spacecraft, *Space Science Reviews*, 71, 79-124.

Hamamatsu Photonics K.K. (2021). MCP assembly, *Technical sheet,* Drawing No. AF2226-A286B.

Hathaway, D. H. (2014). The Solar Wind, https://solarscience.msfc.nasa.gov/SolaWindogov/SolarWind.shtml.

Hotta, M., Adachi, T. (2014). Two rotating electric fields mass analyzer, *USA Patent 9,570,279.*

Hundhausen. A. J., Asbridge, J. R., Bame, S. J., Strong, I. B. (1967). Vera satellite observations of solar wind ions, *Journal of Geophysical Research,* 72 (7). 1979-1987.

Ipavich, F., (1997). Early data from the solar wind ion composition spectrometer, *ACE news #7, https://izw1.caltech.edu/ACE/ACENews_Archives.html*

Kallenbach, R., Ipavich, F. M., Bochsler, P., Hefti, S., Hovestadt, D., Grunwaldt, H., et al (1997). Isotopic composition of solar wind neon measured by CELIAS/MTOF on board SOHO, *Journal of Geophysical Research*, 102(A12), 26,895-26,904.

Kasper, J. C., Abiad, R., Austin, G., Balat-Pichelin, M., Bale, S. D., Belcher, J. W. et al. (2015). Solar wind electrons alphas and protons (SWEAP) investigation: Design of the solar wind and coronal plasma instrument suit for solar probe plus, S*pace Science Reviews,* DOI 10.1007/s11214-015-0206-3

Kramer, J. and Le Poole, J. B. (1954). A new high frequency mass spectrograph, *Industrie Chimique Belge,* 19, 705- 706.

Leske, R. (1997). First data from the cosmic ray isotope spectrometer (CRIS), *ACE news #1, https://izw1.caltech.edu/ACE/ACENews_Archives.html*

Leske, R. (1997). Isotope measurements from the 11/6/97 solar particle event, *ACE news # 5, https://izw1.caltech.edu/ACE/ACENews_Archives.html*

Marsch, E. (2006). Kinetic physics of the solar corona and solar wind, *Living Review, Solar Physics*, 3, 1. [Online Article]: cited [23 December 2021],http://www.livingreviews.org/lrsp-2006-1

Mason, G. M., Gold, R. E., Krimigis, S. M., Mazur, J. E., Andrews, G. B., Daley, K. A, et al, (1998). The ultralow- energy isotope spectrometer (ULEIS)

for the ACE spacecraft, *Space Science Reviews.* 86: 409-448.

Mason, G., Dwyer J. (1997). Early Data from the Ultr-Low Energy Isotope Spectrometer (ULEIS), *ACE news #6, https://izw1.caltech.edu/ACE/ACENews_Archives.html*

Moritani, K., Hotta, M., Nojima, M., Kurumi, S., Suzuki, K., Adachi, T. et al (2018). Method to measure the size distribution of massive cluster ion beams using two rotating electric fields, *Nuclear Instruments & Methods in physics Research*, B, 432, 1-4.

Mukai, T., Miyake, W., Terasawa, T., Hirao, K. (1987). Observations of solar wind ions by interplanetary spacecraft Suisei (PLANET-A), *Journal of Geomagnetism and Geoelectricity*, 39, 377-395.

Neugebauer, M., Liewer, P. C., Smith, E. J., Skoug, R. M., Zurbuchen, T. H. (2002). Sources of the solar wind at activity maximum, *Journal of Geophysical Research,* 107(A12), 1448, doi: 10.1029/200IJA000306, 2002.

Nojima, M. (2017). Imaging mass spectrogram using rotating electric fields mass spectrometer, *Global Journal of Nanomedicine,* 2(5) 84-86.

Nojima M., Anai, Y., Hotta, M., Kurumi, S., Suzuki, K. Adachi, T. (2016). Development of a mass spectrometer using two rotating electric fields, *Journal of Vacuum Science and Technology, B.* 34(3), 03H132-03H132-4.

Ogilvie, K. W., Wilkerson, T. D. (1969). Helium abundance in the solar wind, *Solar Physics*, 8**,** 435-449.

Ohwaki, K., Dake, Y., Toyoda, N. and Yamada, I. (2005). Development of a new cluster size selector, *Nuclear Instruments and Methods,* B, 241, 614-617.

Parker, E. N., (1961). The Solar Wind, *Journal of Research of the National Bureau of Standards, D*, 65D (6), 537- 542.0.

Ryden, B. (2011). Astronomy 825: Radiative gas dynamics, chapter 11, The solar wind, *http://www.astronomy.ohio- state.edu/~ryden/ast825/ch11.pdf.*

Shearer, P., von Steiger, R., Raines, J. M., Lepri, S. T., Thomas. W. Gilbert, J. A., et al (2014), The solar wind neon abundance observed with ACE/SWICS and Ulysses/SWICS, *The Astrophysical Journal,* 789: 60. 1-10.

Von Steiger, R., Wimmer-Shweingruber, R. F., Geiss, v., Gloeckler, G. (1995). Abundance variations in the solar wind, *Advances in Space Research,* 15(7), 3-12.

Von Steiger, R., Vial, J.-C., Bochsler, P., Chaussidon, M., Cohen, C. M. S., Fleck, B., et al (2001). Measuring solar abundances, *http://lib-www.lanl.gov/la-pubs/00796345.pdf.*

Wimmer-Schweingruber, R. F., A., (1998) Solar Wind Isotopes in the May 3, 1998 CME:SWIMS Data, *ACE news #19, https://izw1.caltech.edu/ACE/ACENews_Archives.html*

Zastenker, G., Borodkova, N., (1991). Long-Term Energy and Momentum Flux Fluctuations, *Journal of Geomagnetism and Geoelectricity*, 42, 89-99.

Zurbuchen, T.H., Hefti, S. (1998). First measurement of the solar wind composition with the high resolution mass spectrometers SWIMS, *ACE news #10, https://izw1.caltech.edu/ACE/ACENews_Archives.html*